Wolfson School of Mechanical, Electrical and Manufacturing Engineering

Individual Project
Final Report

ID Number: F133245

Programme: Robotics, Mechatronics and Control Engineering

Module Code: 23WSC50META

Project Title: Optical sensor for high-precision measurement of axial rotation (roll)

Abstract

Rotation sensors that becoming increasingly important in most technologies used in our day-to-day life. This project develops a system, a fibre optic Sagnac interferometer. The aim of this project is to be able to measure axial rotation to a very high precision. Existing sensors and literature surrounding interferometers is reviewed, and an oscilloscope is used to record data. This data is then used to test and fulfil the aims of this project.

The setup of the interferometer and the calculations for roll are the most important aspects of this project. The Sagnac effect was used with the interferometer to enable it to successfully detect angular velocity which can then be integrated to get roll angle.

Results produced in each test are compared. This showed that the interferometer is able to record intensity and with the use of different equation calculate angular velocity to a very high precision.

Overall, the interferometer was not able to detect the direction of rotation. The system can still detect the roll angle, but due to the lack of direction in the reading the interferometer measures angular distance moved rather than angular displacement (roll).

Wolfson School of Mechanical, Electrical and Manufacturing Engineering

Table of Contents

Wolfson School of Mechanical, Electrical and Manufacturing Engineering

Project Aims

The main aim of this project is:

'To design, develop, and validate an optical sensor capable of high-precision measurement of axial rotation (roll).'

Project Objectives

The objectives of the project have been laid out in order to provide guidance and clarity. Furthermore, they allow for effective progress tracking. The objectives are:

- Research on all the existing optical sensors that can measure roll in detail and compare them using a Pugh matrix.
- Propose detailed designs (fundamental formulas, CAD, optical diagram etc.).
- Design and build the optical setup using the sensor chosen.
- Test and record data for roll angle measurements.
- Validate the system with a calibration rotation stage.

1   Introduction

One of the most unique features of measuring rotation is its ability to be done without an outside reference point, unlike speed. High precision rotation measurements developed for the precision control of planes were not initially possible. In the 1970s, active laser interferometers were used, however, these were big, fragile, and not portable [1]. By the 1980s, fiber optic gyroscopes (FOGs) became widely used, however, these were expensive and difficult to manufacture [1]. The most recent rotation sensors are small, inexpensive, and commonly used in commercial cell phones. These solid-state proof masses originate from a silicone substrate.

The future of modern rotation sensing appears bright, boasting a diverse array of sensor choices catering to various applications [1]. These sensors exhibit remarkable capabilities, detecting subtle alterations in Earth's rotation velocity or swiftly accommodating rapid motions at multiple radians per second with exceptional precision [1].

Their utilization spans across a multitude of sectors including vehicle and aircraft navigation, smartphone tilt control, and the emerging field of rotational seismology, focused on studying rotations during seismic events. As their affordability increases and sensitivity advances, rotation rate sensors are increasingly indispensable for structural health monitoring purposes [1].

The system to be designed, developed, and validated in this project will aim to provide precise measurements of axial rotation (roll), showcasing areas where modification is possible for improvements. It will be useable in environments that require high-precision roll angle detection. The effectiveness and robustness of the sensor will experience comprehensive evaluation to ensure its applicability across diverse real-world settings demanding accurate rotational measurements. This project will strive to advance optical sensing technology while catering to the distinct requirement for high-precision axial rotation measurement.

1.1   Report Structure

This report has been divided into different sections to display the progress made in an organised and efficient manner. It consists of the following sections:

- **Background**
  Summarises the important findings made during the literature review as well as new knowledge learned throughout the course of this project.
- **Interferometer**
  Outlines how the interferometer works, and the improvements made in recent years.
- **Design**
  Outlines the plans made to build an interferometer and how the components and apparatus would be setup. Including diagrams and calculations involving fibre length, rotation speed and phase change relationships.
- **Building**
  Outlines the parts used and the CAD drawings for the setup, includes the assembly of the full rig which has all the fibre sensors, light source, and pendulum etc.
- **Testing**
  Outlines the testing and development of the interferometer and how it measured the axial rotation of an object.
- **Results**
  Discusses the data produced by the interferometer. Summarises the equations of intensity I(t) for the Sagnac interferometer, and how intensity I(t) is used to get phase (t) or frequency f(t) and get angular velocity ω (t) and the tilt or roll angle.
- **Conclusions and further work**
  Summarizes key findings and suggests potential future research directions or actions based on those findings.

2   Background

2.1   Existing solutions to measure roll

2.1.1   Gyroscopes

Gyroscopes are a very important tool to measure angular velocity. They are two types of gyroscopes, mechanical gyroscopes, such as spinning wheels, and solid-state options like MEMS gyroscopes. The gyroscopes work together with accelerometers to determine an object's 3D orientation. Making use of the Sagnac effect, the gyroscope effectively determines angular velocity. Through Integration as shown in Equation 1,you can acquire the roll angle of the object [2].

$$(\emptyset = \int (\omega)dt) \tag{1}$$

where: $\emptyset$　　　is the Roll angle (radians)

ω　　　is the angular velocity (rad/s)

Amongst the gyroscopes, the MEMs gyroscope stands out as the most frequent choice for measuring angular velocity, which is then used to calculate roll angle of the object. These gyro sensors can be very small, comparable in size to a human hair. When the object is rotated, a minute resonating mass within them shifts with changes to angular velocity as illustrated in Figure

1. This motion is converted to low-current signals, which are then amplified and interpreted by a microcontroller to determine the angular velocity and roll angle accurately [3].
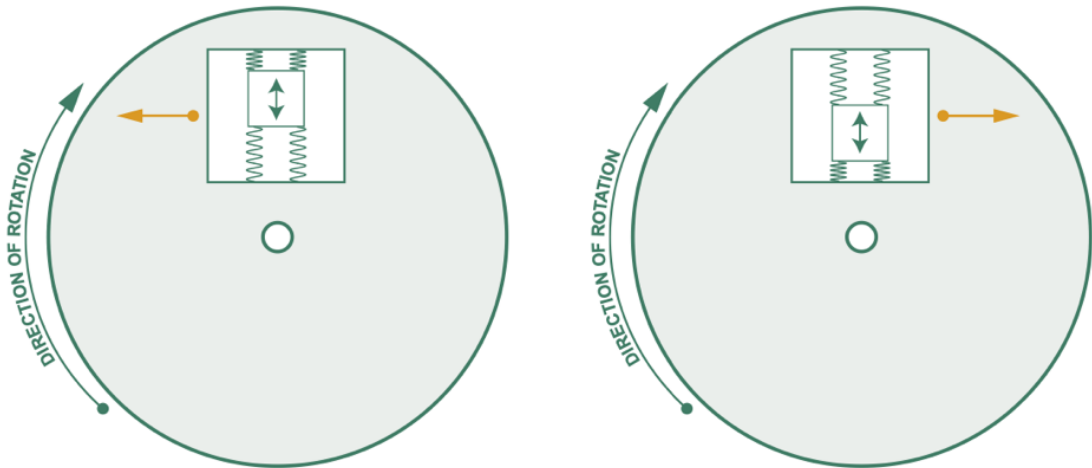

Figure 1 – the silicon mass suspended in the frame during a rotation. [3]

2.1.2   Inclinometers

Inclinometers are commonly used instruments for roll angle measurements. They have a wide range of uses across various industries, including rail traffic, aerospace, gesture control and industrial automation. As things start to modernise and progress into the information technology era, the demand for precise inclinometers become increasingly urgent[4].

Using Newton's second law, which states that an object only experiences gravity when placed horizontally without any external forces acting upon it, Inclinometers calculates the roll angle of an object by decomposing gravitational acceleration which shows the roll angle [4]. Old-fashioned protractor level inclinometers rely on human-operated measurements, which led to potential inaccuracies, as shown in Figure 2. However, the electronics inclinometers use pendulum characteristics, and they come in liquid, solid or gas forms. The only drawback is they often require a stable condition for accurate readings [4].
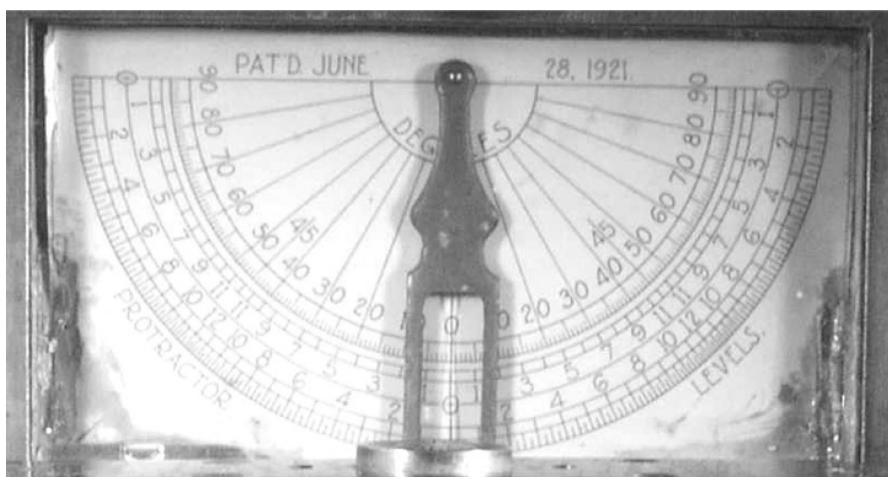

Figure 2 – a protractor level inclinometer [5]

Fibre optic inclinometers which are used to monitor static roll angles of civil engineering structures use transmissive grating panels and optical fibres for measurements. However, they are limited by their fine range for roll angle measurements [4].

2.1.3   Laser Interferometry

The origin of laser interferometry dates back to 1801, when the well-known British Scientist Thomas Young carried out his novel two-slit interference experiment. Since this pivotal work, a diverse array of laser interferometers has been developed. They have been put in different categories based on if they use wavefronts of amplitude splitting principles [6].

The wavefront splitting interferometers shown by Young's two slits experiment, Lloyd's mirror experiment and Rayleigh interferometers, are used in spatial light devices which are used divide the incoming light wavefront from a point to a narrow slit [7].

Amongst these, the Sagnac interferometer stands out as one of the most commonly used interferometers, where both light beams traverse the same pathway.

In the Sagnac interferometer, a beam of light is directed towards the beam splitter, which divides it into two beams moving in opposite directions, usually within a closed circular path as illustrated in Figure 3 [8]. Under normal conditions when the interferometer is stationary, these beams maintain a constant phase coherence, resulting in no interference. However, when there is a rotation introduced to the system, one beam travels a greater distance than the other, causing them to become 'out-of-phase', which leads to the formation of interference patterns. Scientists then use these interference patterns to precisely measure the roll angle of the object.
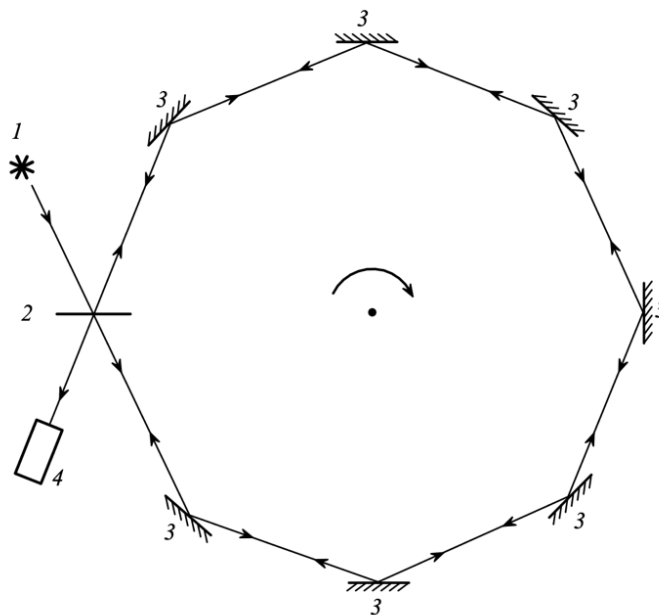

Figure 3 – Sagnac interferometer: 1 - light source, 2 - beam-splitter, 3 - mirrors, 4 - photodetector. The arrow in the middle shows the direction of interferometer rotation [9]

2.1.4   Digital Holography

Digital holography captures a hologram of an object, usually using lasers. The laser splits into two beams, one is the reference beam, and the other is the object beam. These beams then combine and interfere, forming a hologram on a light-sensitive detector [10]. Using computer programs, this hologram is then turned into a 3D image of the object, as shown in Figure 4. When you acquire the 3D image, you can study the object's orientation to obtain the roll angle [11].

Some researchers have worked on this. Matsushima et al. proposed a way to find the roll angle of an object by rotating and filling in missing parts of the image. However, their research and method

doesn't fully account of the object's rotation. Pan et al. presented a method to recreate images on rotated planes by rotating the object's wavefronts. However, their method only considers rotation along one axis, and they focus on describing the results that have been obtained rather than analysing them in detail [12].
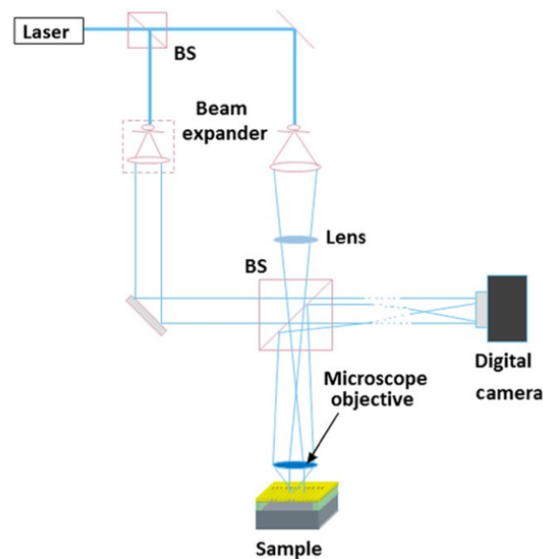

Figure 4 - Optical setup for digital holography [13]

2.1.5   Optical Encoders

In robotic systems, rotary encoders are essential as rotations sensors because they require high resolutions, precision, response rates and compact sizes. These encoders have achieved notable accuracies, with uncertainties as low as 0.005 inches for the German national Institute standards and 0.05 inches for the Japanese Agency of Industrial Science and Technology [14]. Whilst these encoders are favoured mainly for their compact size, lightweight, and high response frequencies, and resolution, they are impractical for small batch production due to the need for an original code disk regardless pf production volume [14].

The rotary encoder operated using a scale grating inspire by the spider's web structures, designed with a circular cross-grid graduation. This grating, as shown in Figure 5, consists of periodic patterns in both circular and angular directions, with a large spacing on the outer circle and smaller spacing on the inner circle. The grating's patterns are a result of blending bright areas together denoted as p_x and p_y along the angular and circular directions, respectively[16]. They are two types of gratings, amplitude and phase grating. An amplitide grating with transparent and opaque areas is used in this this case. Roll angle is calculated from the angular direct grating pattern, whilst the displacement of an object along a circular pathis determined from the circlular direction pattern[16].

Changes in the alignment ring is detected by an optical microscope, which indicate the oddity of the scale grating. A dual-head scanning unit, facilitates photoelectric reading of the roll angle and circular displacements. This component has two scanning heads arranged perpendicularly, with the primary head which detects relative movement in the angular direction and the second head detecting movements in circular directions [15].
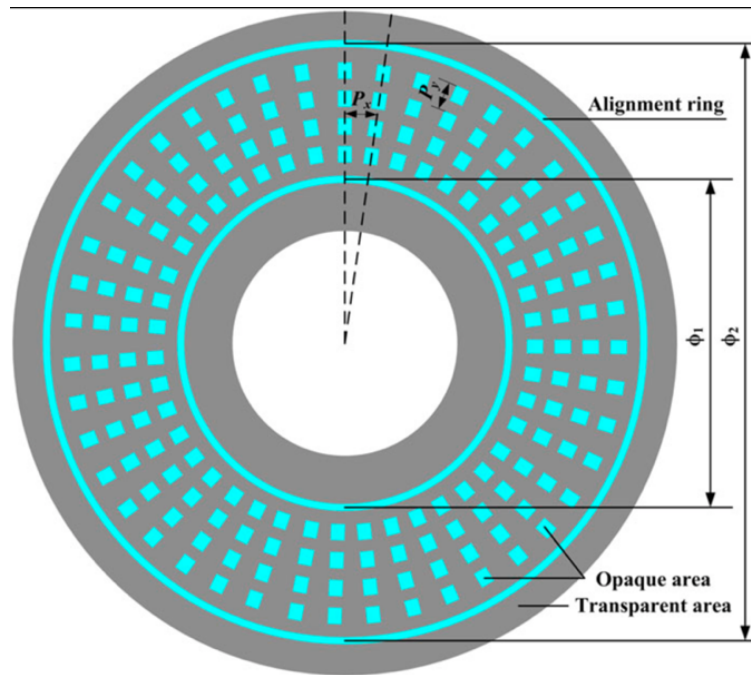
Figure 5 - Schematic pattern of the scale grating for the rotary optical encoder [15]

2.2 Comparison

After carefully analysing the data gathered during the background research, the information was compared using a Pugh matrix, resulting in rankings as shown in Table 1. Following the evaluation of rankings, the Interferometer appeared to be the most favourable option for progression.

Criteria	Gyroscope	Inclinometer	Interferometer	Digital Holography	Rotary Encoders	Baseline	Weighting
Resolution	1	1	3	2	2	0	4
Accuracy	1	1	3	2	1	0	4
Cost	-1	-2	1	-1	-2	0	5
Complexity	-3	-1	-1	1	-1	0	5
Robustness	3	1	-1	-1	-1	0	2
Integration	2	1	-1	-2	3	0	1
Power Consumption	2	2	2	1	2	0	1
NET SCORE	5	3	6	2	4		
RANK	2	4	1	5	3		
CONTINUE?	Maybe	No	Yes	No	Maybe		

Table 1 – Pugh Matrix

3 The Sagnac Interferometer

3.1 How does the Sagnac Interferometer work?

The first ring laser gyroscope was introduced in 1963 marked the beginning of ongoing research into similar devices. The initial experiments, which laid the groundwork for these events to occur was conducted by Sagnac in 1911 [16]. Sagnac's experiments involved rotating the whole interferometer, including the mirrors, light source and the detectors around the perpendicular axis passing through its centre. This experiment involved two overlapping beams to traverse the interferometer, one moving in the clockwise direction and the other counter-clockwise. The rotation of the interferometer causes one beam to travel a shorted distance compared to the other, which resulted in a fringe shift in the interferometer proportional to the angular speed of rotation [16]. This setup is shown in Figure 6, this involves corners such as A moving with a linear speed.
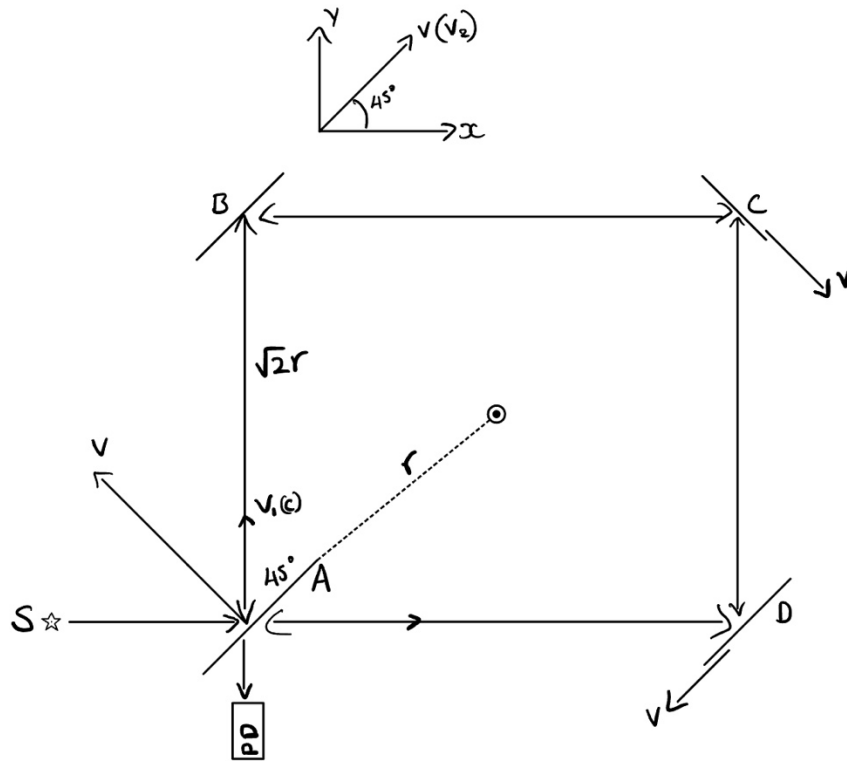

Figure 6 – Sagnac interferometer setup: S - light source; A - beam-splitter; B, C, D – mirrors; PD - photodetector. The arrow (V) shows the direction of interferometer rotation at a certain velocity.

Mirror B is in motion away from A, therefore, using logical reasoning, we can find the duration of light's journey from A to B by using Equation 2. For the calculation of the time required for a full clockwise rotation, Equation 2 should be multiplied by '4', and '-4' for an anticlockwise rotation [16].

$$t_{AB} = \frac{Distance\ from\ A\ to\ B}{Relative\ Speed} = \frac{2\sqrt{r}}{(v1)-(v2)} = \frac{2\sqrt{r}}{c-\frac{v}{\sqrt{2}}} = \frac{2r}{\sqrt{2}c-v} = \frac{2r}{\sqrt{2}c-\omega r} \tag{2}$$

where: c is the speed of light (m/s)

      v is the mirror moving velocity (m/s)

r is half the diagonal of the square (m)

ω is the angular velocity (rad/s)

To determine the difference in time required for the recombination of the two beams, subtract the duration of the counter-clockwise rotation from that of the clockwise rotation. This is necessary because the interferometer is rotating in a clockwise direction, as illustrated in Equation 3.

$$\Delta t = \frac{8r}{\sqrt{2}c - \omega r} - \frac{8r}{\sqrt{2}c + \omega r} = \frac{16r^2\omega}{2c^2 + \omega^2 r^2} = \frac{8r^2\omega}{c^2} \qquad (3)$$

(We can disregard $\omega^2 r^2$ due to its insignificance relative to c^2)

Using the formula for the fractional displacement of fringes which is shown in Equation 4, you can get Equation 5 after substituting all the other equations.

$$\Delta N = \frac{\Delta t}{\tau} \qquad (4)$$

where: ΔN is the number of fringes formed

Δt is the time taken for the two beams to recombine (s)

τ is the period of monochromatic light (s)

After substituting the equations:

$$\Delta N = \frac{8r^2\omega}{c\lambda} \quad \text{or if we express this in terms of area(A)} \quad \Delta N = \frac{4A\omega}{c\lambda} \qquad (5)$$

where: A is the area of the loop (m^2)

r is the radius (m)

λ is the wavelength of the light or laser used (m)

c is the speed of light (m/s)

ω is the angular velocity (m)

The actual path difference is twice this amount so with a little manipulation we can find the phase difference between the two beams using Equation 6 [17].

$$\emptyset = \frac{8\pi A\omega}{\lambda c} \qquad (6)$$

where: $\emptyset$ is the phase difference for the 2 beams (radians)

The results have been confirmed through experimental validation. Notably, Michelson and Gale used this approach the Earth's angular velocity [16]. However, the earlier logical analysis falls short as it assumes velocities surpassing the speed of light, which contradicts the principles of relativity. Moreover, given the system's acceleration, it seems that the general relativity would take preference [16].

3.2   The fiber optic interferometer

The ring laser interferometer was first used in commercial aircrafts with the introduction of the Boeing 757 [17]. Similarly, the optical fiber interferometer uses an external light source, basically making Sagnac's single-loop configuration into a multi-turn loop. This multi-turn loops extends the optical delay of the interferometer which enhances the sensitivity of the interferometer. Vali and Shorthill first showcased the fiber optic interferometer in 1976 [17]. This was initially used for aircraft stabilization and heading control systems unlike the ring laser interferometer which was used for inertial navigation. However, significant advancements have occurred in the past decade, with the fibre optic interferometer demonstrating sensitivity and accuracy that exceeds the of the competing rotation measurement technologies. The fiber optic interferometer also possesses mechanical ruggedness due to its absence of moving parts [17].

Equation 5, which relates to light transmission in a vacuum loop, becomes modified when the vacuum path is replaced with optical fiber, leading to slight adjustments in the velocities of light in each direction as shown in Equation 7 [17].

$$c\pm = \frac{c}{n} \pm \omega r \alpha \qquad\qquad (7)$$

where: n is the effective index of the fibre.

r is the radius (m)

ω is the wavelength of the light or laser used (m)

c is the speed of light (m/s)

α is the relativistic drag imposed by the dielectric medium (m/s)

If we replace the delays with velocities, as previously done, we arrive at the identical expression for the phase delay in relation to rotation rate, as illustrated in equation 6 [17].

4   Design

4.1   Components and setup design

A fiber optic interferometer requires several key components. These include beam splitters or fibre couplers, a laser source, a photodiode, and the fiber optic cable as shown in Figure 7.
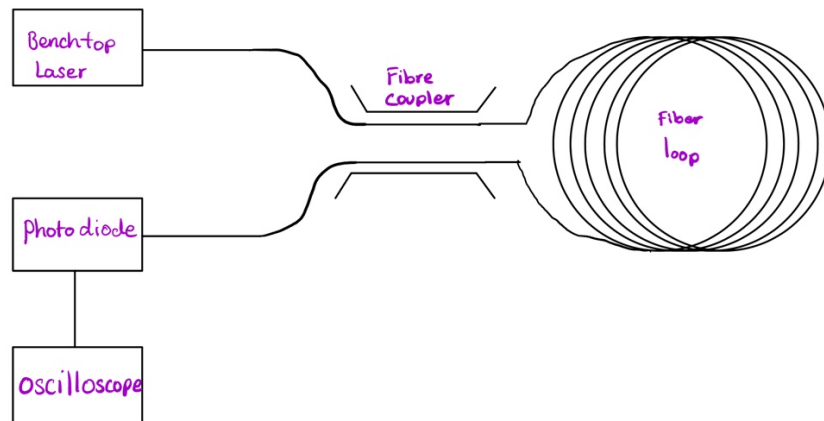

Figure 7 – Shows how the fiber optic interferometer would be setup and all the component required

4.1.1   Lasers

The most common choice for lasers used in interferometers is the Helium-Neon(He-Ne) laser due to its affordability and capability to generate a continuous and visible beam. They usually operate at 633nm, He-Ne offers modified versions catering to various and infrared wavelengths [18]. Argon lasers cost more than the He-Ne laser, but they produce a significantly larger output. Additionally, laser diode systems are used, they offer a wide spectrum from infrared to the violet religion. However, laser diodes have drawbacks such as divergent and astigmatic output beams [18].

It is possible to encounter challenges with laser sources. The most common one arises from the high degree of coherence of the laser, which often leads to the generation of random diffraction patterns, commonly referred to as spatial noise. Another concern in the formation of unwanted interference fringes due to the presence of stray light [18]. Furthermore, optical feedback also presents a significant concern, as light reflected back to the laser can cause fluctuations in its power output and potentially alter its frequency [18]. One common solution for these problems is using an optical isolator. It prevents the reflected light from re-entering the laser system and separates the laser source from the external reflection and helps maintain power output and frequency, thereby optimizing performance and mitigating disruptive effects.

4.1.2   Fibres

Single mode optical fibres tend to be the most common choice in fibre optic cables due to their amplified sensitivity [19]. This sensitivity stems from the unique capability to facilitate the construction of a guided wave interferometer within the fibre itself, which enables precise measurements of very small phase variations in transmitted light across the designated area of measurement. In a practical scenario, the stability of the single-mode fibre is very important, especially when using highly coherent light sources with very small phase noise to fully exploit their sensitivity [19].

4.1.3   Photodiodes

The photodiode is a semiconductor device that converts the light energy given into electrical current or voltage. This happens when the photons strike the semiconductor material in the photodiode, they transfer energy to the electrons causing them to break from their atomic bonds and create hole pairs [18]. These hole pairs result in the flow of a current within the photodiode which can then be measured as a voltage across terminals. The voltage produced will be proportional to the light intensity [18].

4.1.4   Polarization wheel

In a fibre optic interferometer, the precision of measurements might be compromised because of the polarization of light induced by factors such as temperature fluctuations or mechanical stress. Polarization is a phenomenon that occurs when the electric field vector of the light waves oscillates in a particular direction, which can arise through mechanisms such as scattering or reflections [20].

The presence of the polarized light can lead to unwanted interference patterns with the interferometer dur to the way the components in the interferometer are arranged. To mitigate this problem, a polarisation loop is used in the setup to ensure that the light maintains a consistent phase relationship as it propagates through the fiber, therefore minimizing the impact of the measurement's accuracies caused by the polarization of light [20].

4.2   Calculations involving the fiber loop

One of the main elements within the interferometer's setup is the fibre optic cable. The interferometer which has a very high level of sensitivity to accurately measure very small angles with a high precision. The sensitivity of the interferometer correlates directly with the number of rotations of the fiber loop. Essentially, the sensitivity of the interferometer is calculated by the derivative of the phase shift with respect to angular velocity. Other factors, including the loop's area and the wavelength of light used also influences the interferometer's sensitivity.

Two configurations for the coil setup were examined. The first configuration, illustrated in Figure 8, shows the fiber optic cable coiled in a cylindrical shape with loops stacked upon each other, each maintaining a consistent radius of 0.15m. The second configuration, as shown in Figure 9, shows the fiber optic cable coiled with incrementally increasing radii. The smallest loop begins with a radius of 0.01m, progressively increasing by 0.0015m with each subsequent loop.
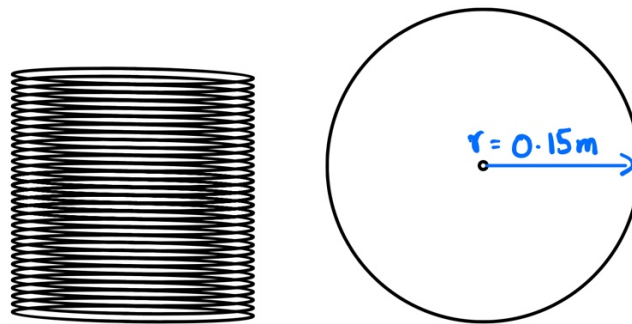

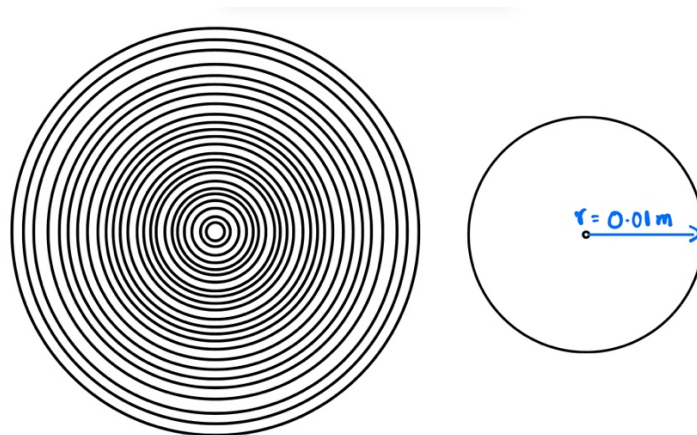Figure 8 – first idea to setup the coil (coiling it up into a cylinder)

Figure 9 – second idea to setup the coil (increasing the radius of the coil by a bit for every loop)

Using Equation 5, we can determine the required length of fiber optics to achieve optimal sensitivity for the interferometer. By ensuring a minimal frequency for the laser to complete one loop, the length of fiber optics can be calculated.

In the first setup, using Equation 5, and assuming we use a laser with a wavelength of 1300nm and a fiber refractive index of approximately 1.5, an angular velocity of 920 rad/s and a frequency of 145 Hz for the laser's loop traversal is derived to obtain one fringe. Considering an estimated setup of 100 coils, the laser's loop frequency amounts to approximately 1.45 Hz, indicating high

sensitivity of the interferometer. Using the formula for circumference, it is found that the first setup needs approximately 0.95m of fiber optics for one loop, therefore requiring around 95m of fiber optic wire for 100 loops.

In the second setup, under identical assumptions as those applied in the first setup and with an equivalent number of coils, an angular velocity of 23 rad/s and a frequency of 4 Hz are calculated for the laser's complete loop traversal to attain one fringe. This suggests a lower sensitivity compared to the first setup. Moreover, the second setup may introduce inconsistencies in the optical path length among the loops, potentially resulting in phase differences and obscure interference patterns. Therefore, the first configuration appeared to be the preferred choice for the interferometer setup.

5   Building the Interferometer

5.1   Pendulum for rotation measurements

The chosen method for measuring the roll angle of an object in the Interferometer involves utilizing a torsional pendulum. Unlike a conventional pendulum, which oscillates in a vertical plane, the torsional pendulum rotates around an axis, as illustrated in Figure 10.
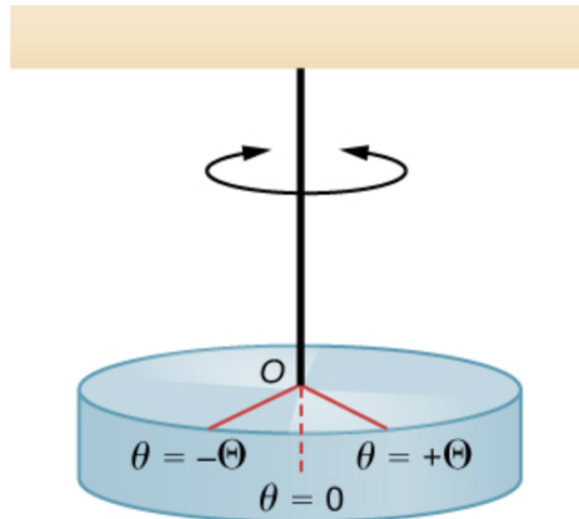

Figure 10 – Torsional Pendulum [21]

In Equation 8, the restoring torque is represented as directly proportional to the angular displacement. The negative sign indicates that the restoring torque opposes the increase in angular displacement [21].

$$\tau = -\kappa\theta \tag{8}$$

where: θ is the angle of rotation of the pendulum (rad)

κ is the torsional constant (kappa) of the wire (Nm/rad)

τ is the torque (Nm)

By setting Equation 8 equal to the total torque, derived from the product of inertia and angular rotation, the period (T) of the pendulum can be calculated, as illustrated in Equation 9 [21].

$$T = 2\pi\sqrt{\frac{I}{\kappa}} \tag{9}$$

where: I is the moment of Inertia (kgm^2)

Torsion and torque are quite similar in mechanics, with torsion representing the twisting deformation of an object in response to applied torque. When a solid rod experiences torsion, it undergoes shear strain, while the application of torque induces shear stress on the solid rod [22]. The relationship between torque and shear strain can be explained using some equations. By using Equation 10 to calculate shear strain and Equation 11 to determine shear stress, we can establish a relationship between torque and shear strain. By making the radius (r) the subject of the formula in both equations and equating them, Equation 11 can be formed as the relationship between torque and shear strain [22]. This analytical approach reveals the basic relationship between torsion, torque, and the resulting shear strain.

$$\gamma = \frac{r\,\theta}{L} \tag{10}$$

where: θ is the angle of twist (rad)

      γ is the shear strain

      L is the length of the rod (m)

      r is the radius (m)

$$\kappa = \frac{T}{\theta} = \frac{\pi r^4 G}{2L} \tag{11}$$

where: T is the torque (Nm)

      G is the shear modulus (Pa)

      κ is the torsional constant (kappa) of the wire (Nm/rad)

The chosen wire for the pendulum in this study was tinned annealed copper (16SWG), characterized by a radius of 0.815 mm and a length of 40 cm. Tinned copper typically has a shear modulus of approximately 45.402 GPa. Using Equation 11, the torsional constant was calculated to be 0.0787. Further analysis using Equation 9 revealed that the frequency of oscillations of the pendulum stands at approximately 0.6 Hz. This frequency is notably low, posing a significant challenge to the sensitivity of the interferometer used in the experiment.

5.2 Components for the interferometer

5.2.1 Laser source

The laser that was selected for this project was the Santec TSL510, which is shown in Figure 11, which was readily available in the optics laboratory at Wolfson. While the He-Ne laser are decent, the slightly higher wavelength have lesser attenuation in standard fibres and produce widely separated fringes, which make it possible to measure smaller rotations, Moreover, lasers with higher wavelengths are more readily available compared to the He-Ne laser [23] [24]. The TSL510 used in the labs possess a tuning range of 1260nm to 1680nm. For this project, a wavelength of 1310n, was chosen, which is the most common wavelength used in telecommunications [25].
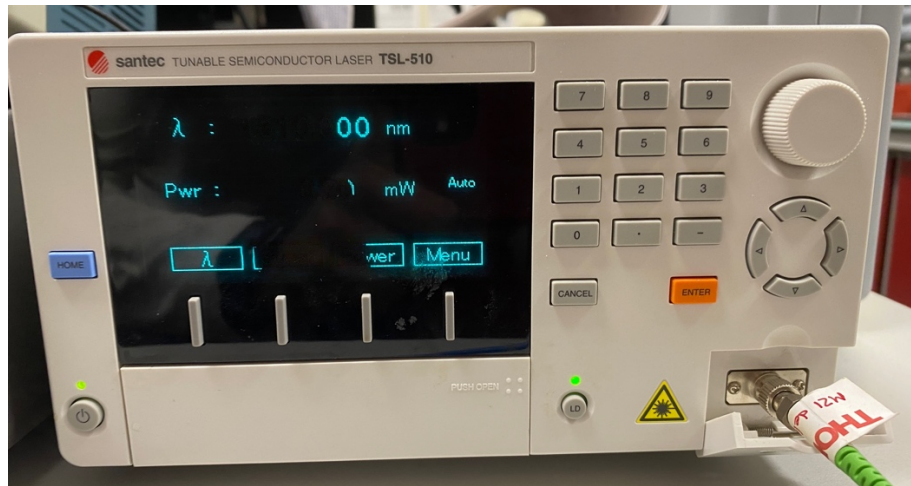
Figure 11 – the Santec benchtop laser

5.2.2   Fibre optic cable

The fibre optic cable that was chosen for this project was the SMF-28-100, which is shown in figure 12. It is characterized as a single mode fibre, offering a low attenuation, reduced splice requirements, wider production tolerance and cost-effectiveness while preserving the coherence and polarization degree and assisting with useful non-linear effects [26]. It has a wavelength rage of 1260nm to 1625nm, and it has an attenuation(max) of ≤0.32dB/km at 1310nm [27]. This minimal attenuation shows the cable's high transmission capabilities, allowing the efficient transmission of signals over a large distance with minimal loss. Since this project is only using about 100 meters of the cable, the signal loss is negligible for this application.

Figure 12 – the SMF-28-100 fibre reel [27]

5.2.3   Photodiode

The experiment uses the PDB570C photodiode as shown in Figure 13, which is readily available in the optics laboratory at Wolfson. Originally the BPX-65 was intended for use with the He-Ne laser. However, due to compatibility reasons, the PDB570C was selected. This photodiode is optimized for 1310nm wavelengths, with a detection range spanning from 1200nm to 1700nm [28]. Its

functionality relies on InGaAs semiconductor material within a PIN structure, effectively transforming incident photons, particularly in the infrared spectrum, into electrical signals.

Figure 13 – the PDB570C

5.2.4 Fibre coupler and circulator

The experiment uses the PMFC-2x2-1310 fiber coupler from Optosun, as shown in Figure 14, which is readily accessible in the optics laboratory at Wolfson. Additionally, the experiment uses the PMCIR-3-A1310 fiber circulator, shown in Figure 15, also conveniently available in the same laboratory. Both components are designed for an operating wavelength of 1310nm, aligning perfectly with the experiment's requirements, and feature FC/APC connectors, consistent with those fitted to the fiber optic cables. The fiber coupler can safely manage power levels of up to ≤300mW, while the fiber circulator is capable of handling power levels of ≤500mW.
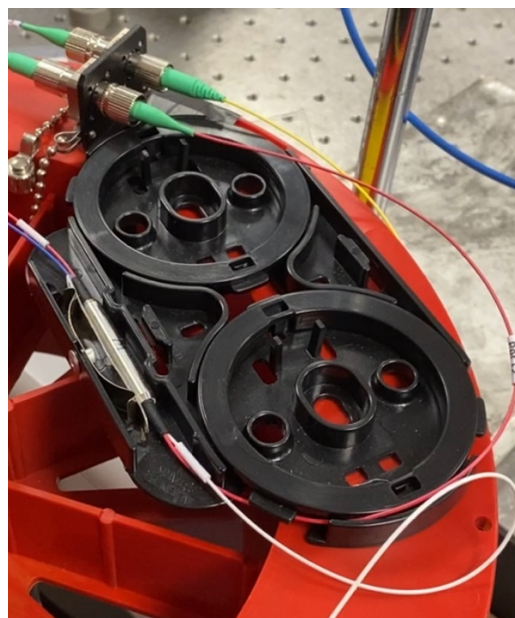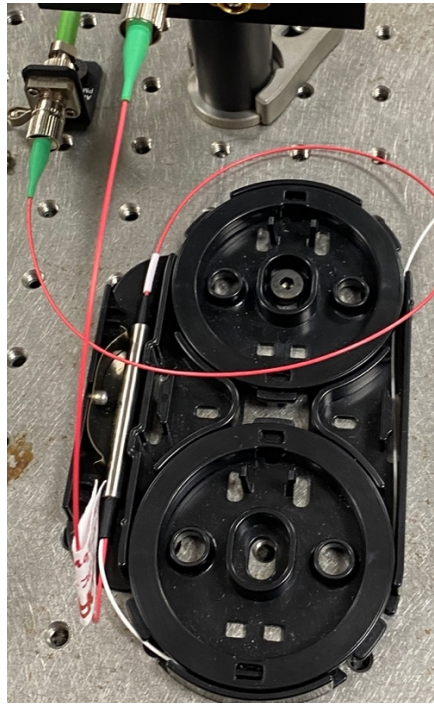

Figure 14 – Fibre coupler

Figure 15 - Circulator

5.3   Final Setup

The torsional pendulum setup used in this project involves the use of a clamp stand, where the tinned copper wire is fixed to the clamp to mitigate any slack. A 3D printed pin as shown in Figure 16 will be combined with the fiber optic reel, as positioned centrally as shown in Figure 17, and secured at the base to prevent any potential movement. The wire is then connected to the pin, and carefully taped to reduce slack in the system. All components, including the fiber coupler, the circulator, and the cable, are polarization maintaining.
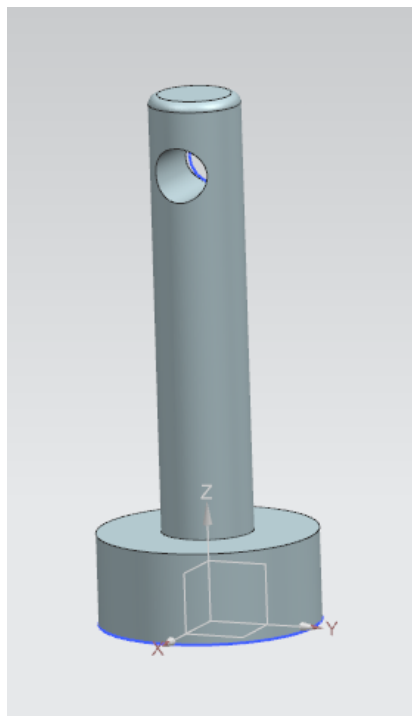
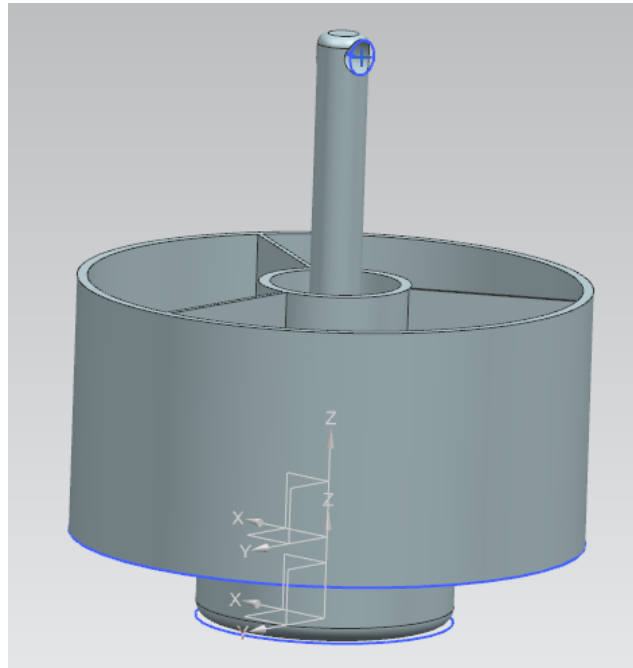

Figure 16 – pin used in the setup

Figure 17 – The pin centred with the reel

The laser source which is connected to the circulator, subsequently linked to the coupler, therefore initiating the split of the laser beam into two different paths before it enters the loops from the coupler. After the beams passes through the entire circuit, they recombine again at the coupler, before traversing back into the circulator. Afterwards, the combined beams are then directed to the photodiode, where the intensity is measured and converted into voltage. This voltage is the shown in the oscilloscope for analysis. The completed setup is shown in Figure 18.
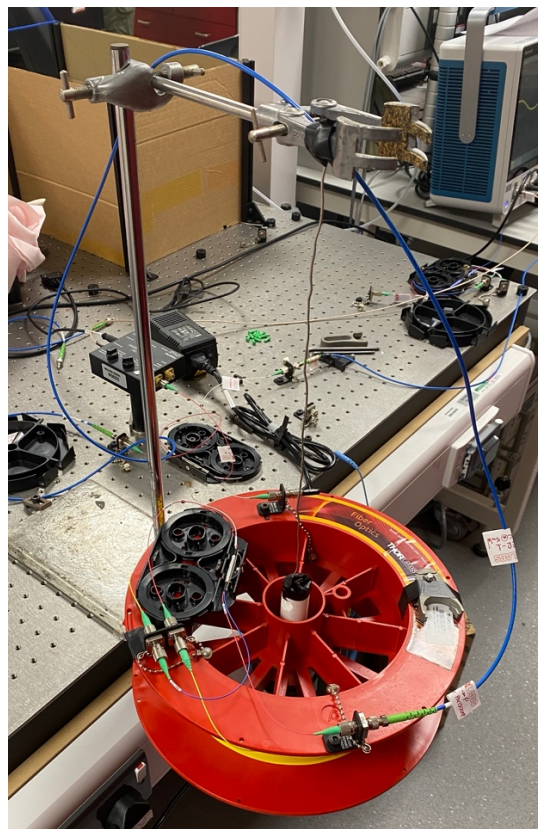

Figure 18 – the complete setup

Consequently, the polarization wheel was excluded from the final setup. This arrangement and components ensure the polarisation is maintained throughout the circuit, therefore removing the need for a polarization wheel.

6   Testing

During the testing phase, as number of assessments were conducted to evaluate the performance of the interferometer in achieving high precision measurements of roll angle. Initially, the torsional pendulum was calibrated so it can be a reliable baseline reference for the experiment. The procedures involved carefully balancing weights on top of the reel, to make sure it was aligned and in level, while monitoring the reading obtained by the photodiode through the oscilloscope.

After the calibration stage, a wide array of validation tests was executed to study the interferometer's performance under different conditions. Varied rotational speeds were applied to the torsional pendulum to measure the interferometer's responsiveness across a spectrum of dynamic scenarios. Particular attention was given to the interferometer's ability to measure subtle rotational movements, and statistical techniques were used to evaluate the precision.

Additionally, the interferometer's long-term stability and drift characteristics were examined over an extended testing period. Continuous monitoring of output readings on the oscilloscope allowed the detection of any indications of drift or deviations from anticipated behaviour over time.

Throughout the testing phase, data acquisition was facilitated through the oscilloscope, with subsequent analysis conducted using MATLAB. The procedures were all documented to ensure there was traceability and reproducibility of the results. The anomalies observed during the tests were analysed and changes were made to the interferometer accordingly.

6.1 Stationary

The first test was assessing the intensity of the light recorded by the photodiode when the interferometer is stationary. This assessment uses port 1 and port 2 on the coupler, as shown in Figure 19. Initially, the assessment was done when the laser was connected to port 1, with an attenuator attached to port 2 to prevent infrared emission from the interferometer. Subsequently to recording the data, the attenuator was switched to port 1 and the laser was connected to port 2 for another round of data collection while the interferometer remained static. These tests aimed to determine the interferometer's consistency in readings in the absence of rotational motion, ensuring the reliability of baseline measurements. Furthermore, these tests included monitoring the interferometer's drift over time to evaluate its long-term stability, which would be relevant for extended measurement tasks.
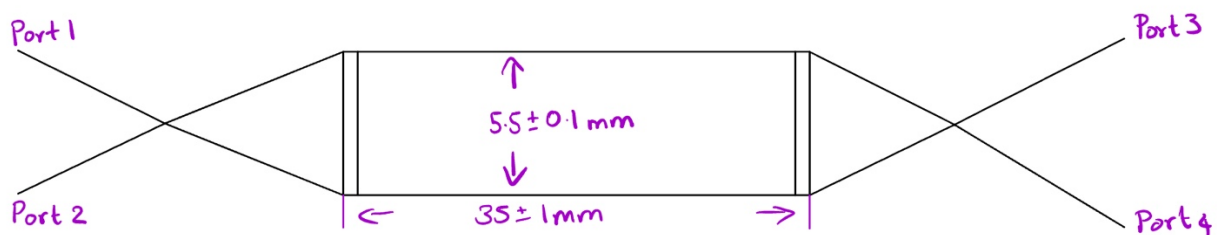

Figure 19 – diagram of the ports in the coupler

6.2   Oscillating

The subsequent tests that were done were used to evaluate the light intensity detected by the photodiode during the oscillation of the torsional pendulum. These oscillations were conducted by varying the frequencies to assess the interferometer's response under different conditions. The data was recorded real-time using an oscilloscope. Additionally, a comparative analysis of the recorded results was done to assess the consistency and accuracy of the interferometer's measurements across different oscillation frequencies. Trends and anomalies observed during the tests were documented for future analysis. Moreover, all the instances where an external factor influence the torsional pendulum's oscillation in the laboratory was recorded, along with their impacts to the interferometer's measurements.

7   Results

The recorded results from the testing phase were thoroughly analysed using MATLAB to assess the interferometer's performance in measuring roll. The first step was transferring all the data recorded using the oscilloscope to MATLAB for further processing. Subsequently, a number of signal processing techniques and equations were used to extract the relevant information related to intensity, phase angle and angular velocity [Appendix A]. Statistical analytical methods, including calculations of the mean and standard deviations were done to gain information about the senor's sensitivity and accuracy in detecting subtle rotational movements. Using a very systematic approach to analyse data from MATLAB, the effectiveness of the interferometer in measuring roll was evaluated, therefore contributing to the realisation of the project's primary objectives.

Figure 20 and Figure 21 shown the results obtained when reading from port 1 and port 2 when the interferometer was stationary, respectively. Figure 22 and Figure 23 shows the results recorded when the interferometer was oscillating with a low frequency. Figure 22 shows results recorded for 4 seconds whilst Figure 23 shows results recorded for 10 seconds. Figure 24 and Figure 25 shows the results recorded when the interferometer was oscillating at a higher frequency. Figure 24 shows results recorded for 4 seconds whilst Figure 25 shows results recorded for 10 seconds.

Initially there was a lot of noise in the recorded signal which was smoothened with the 'movmean' function in MATLAB. The intensity was then used to calculate phase which was then used to calculate the angular velocity. Subsequently, the angular velocity was integrated to get the roll angle for each test. The phase was calculated using the Equation 12, and later the angular velocity was calculated using Equation 13. Through a thorough analysis of Equations 12 and 13, it becomes evident that the phase angle is directly proportional to the angular velocity, while the cosine of the phase demonstrates proportionality to intensity. This correlation is validated by the graphs in Figures 20-25 which consistently uphold these relationships.

After running the tests and processing the data, the system's limitation was identified. The drawback lays in the interferometer's ability to detect the direction of rotation or oscillation. Consequently, rather than subtracting the roll angle for rotations in the opposite direction, it added them cumulatively, therefore ending up with a linear graph as shown in the Figures 20-25. Regrettably, no modifications could be implemented to enable the interferometer to determine the rotation's direction due to lack of time.
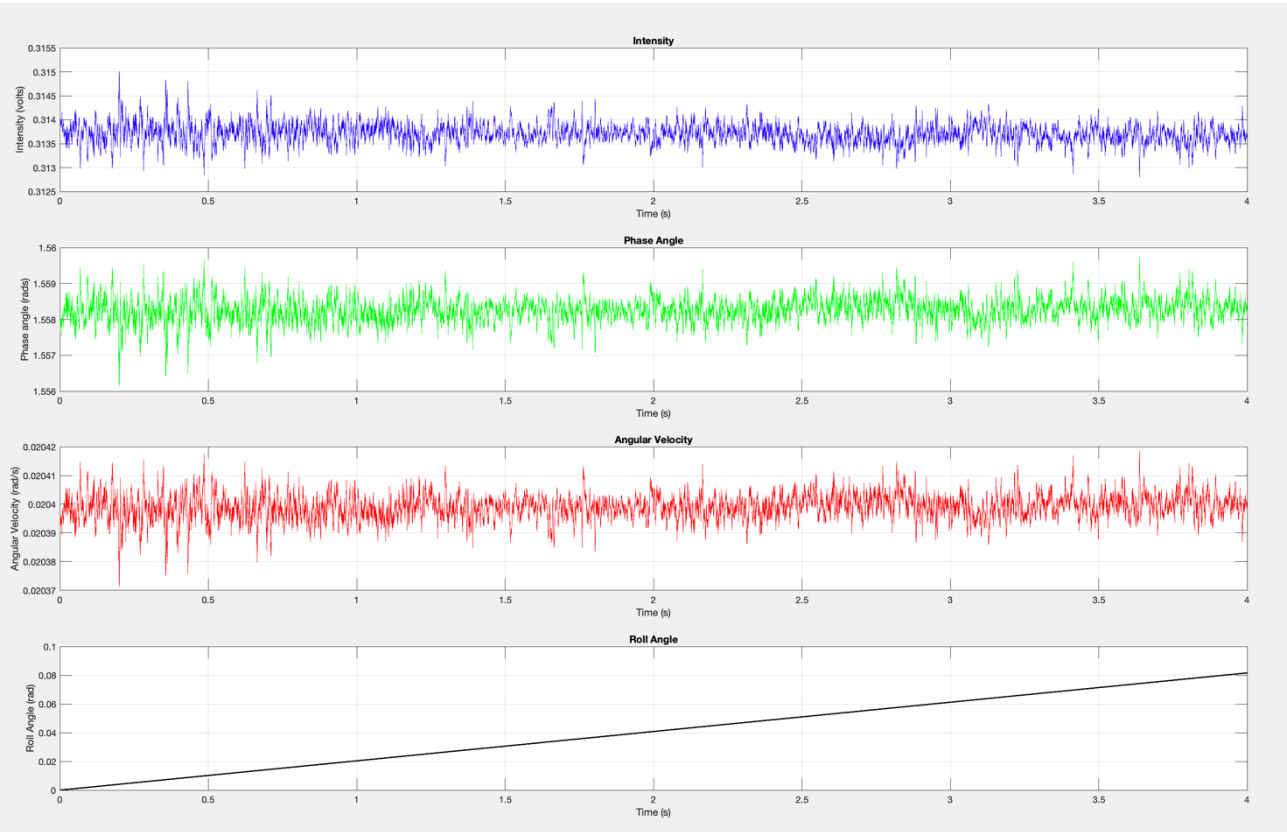
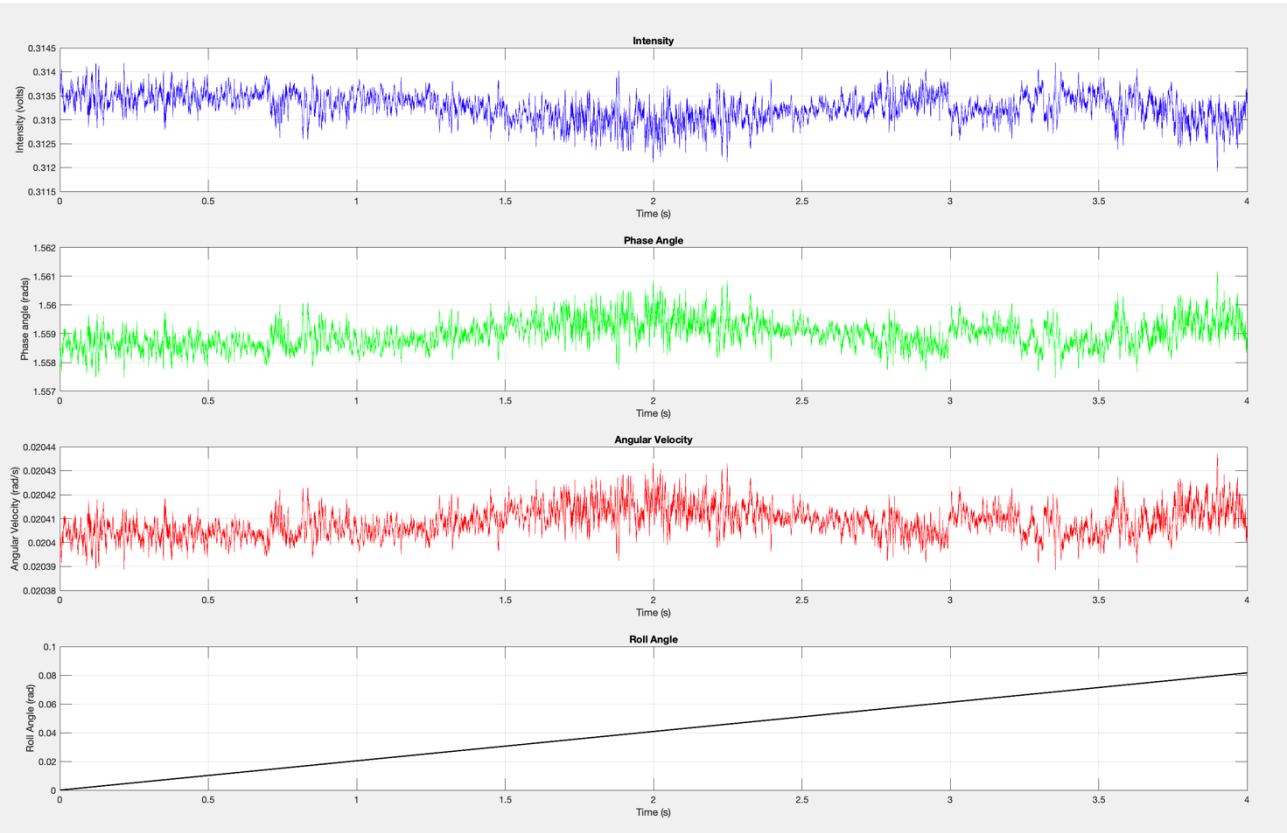Figure 20 – results recorded from port 1 when stationary

Figure 21 – results recorded from port 2 when the interferometer was stationary.
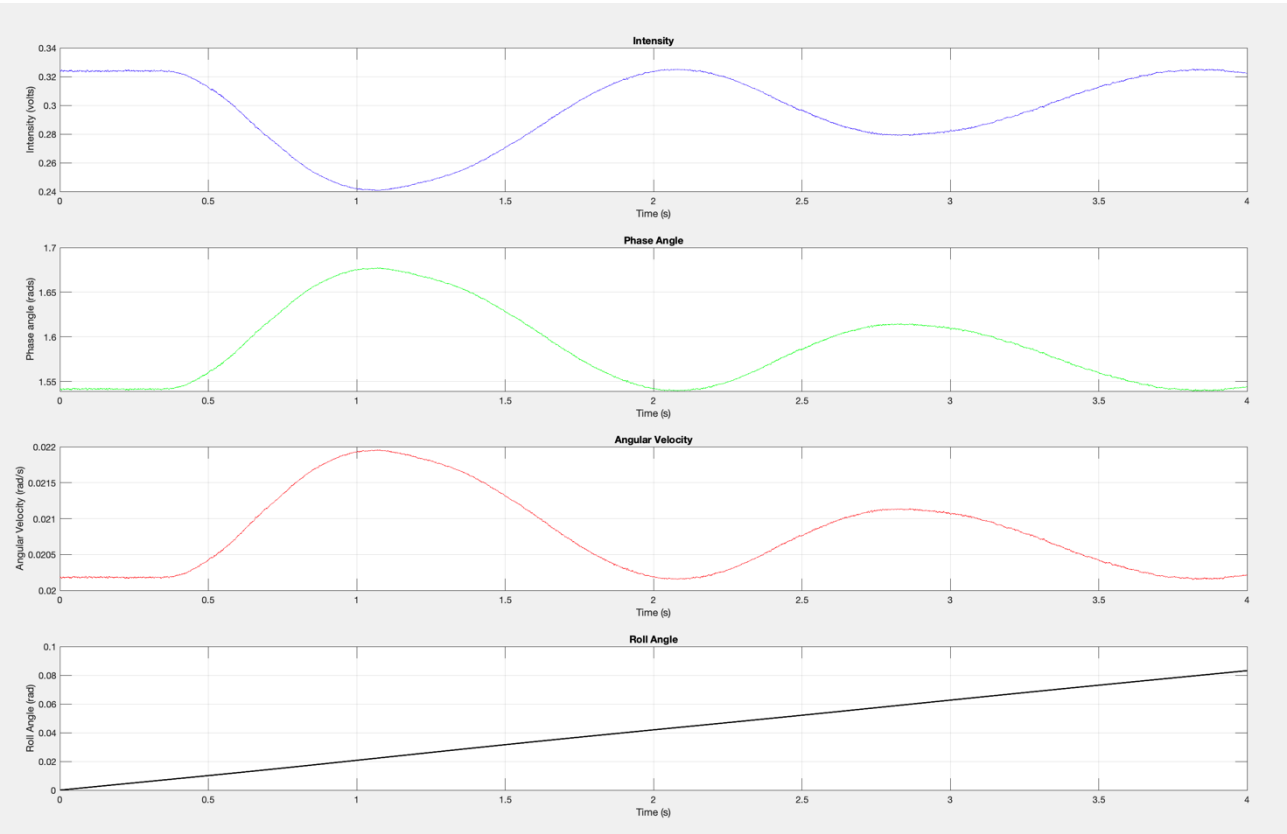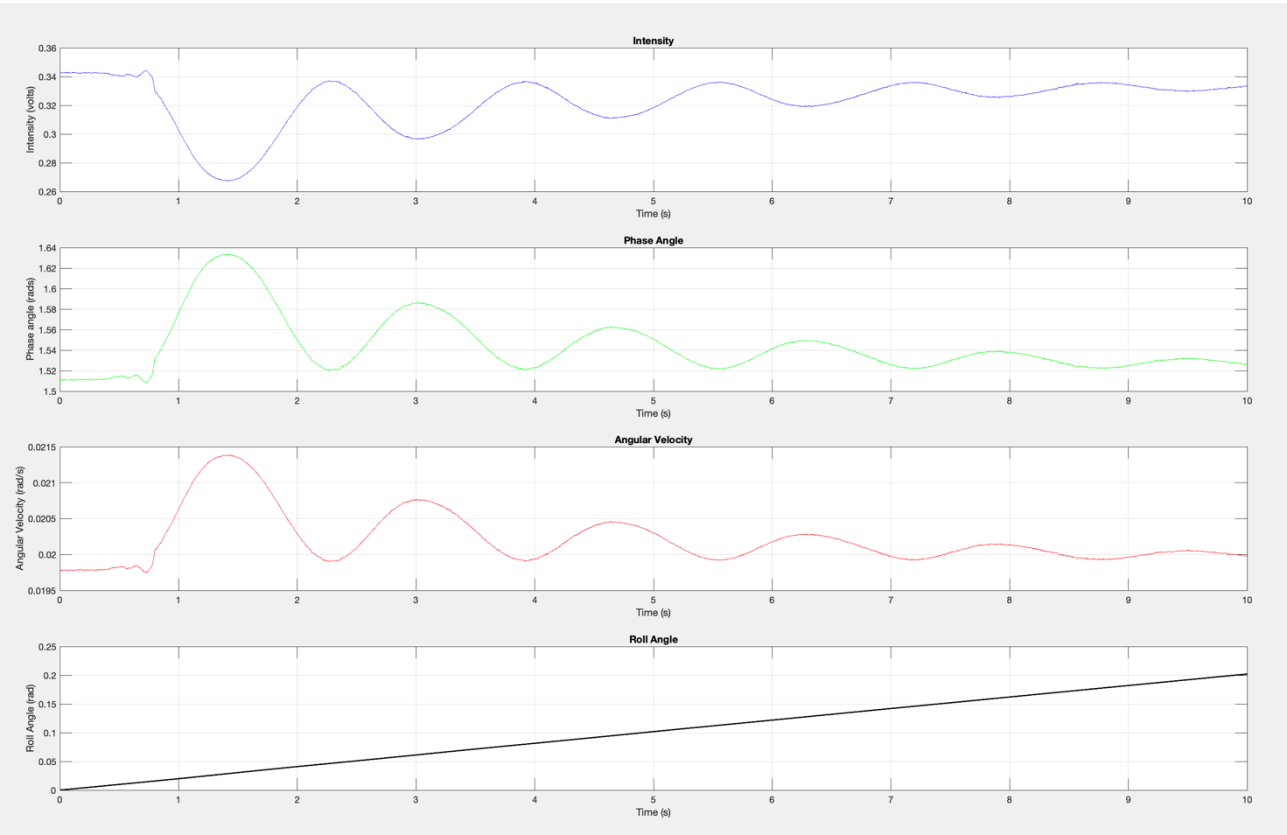
Figure 22 – oscillations for 4 seconds

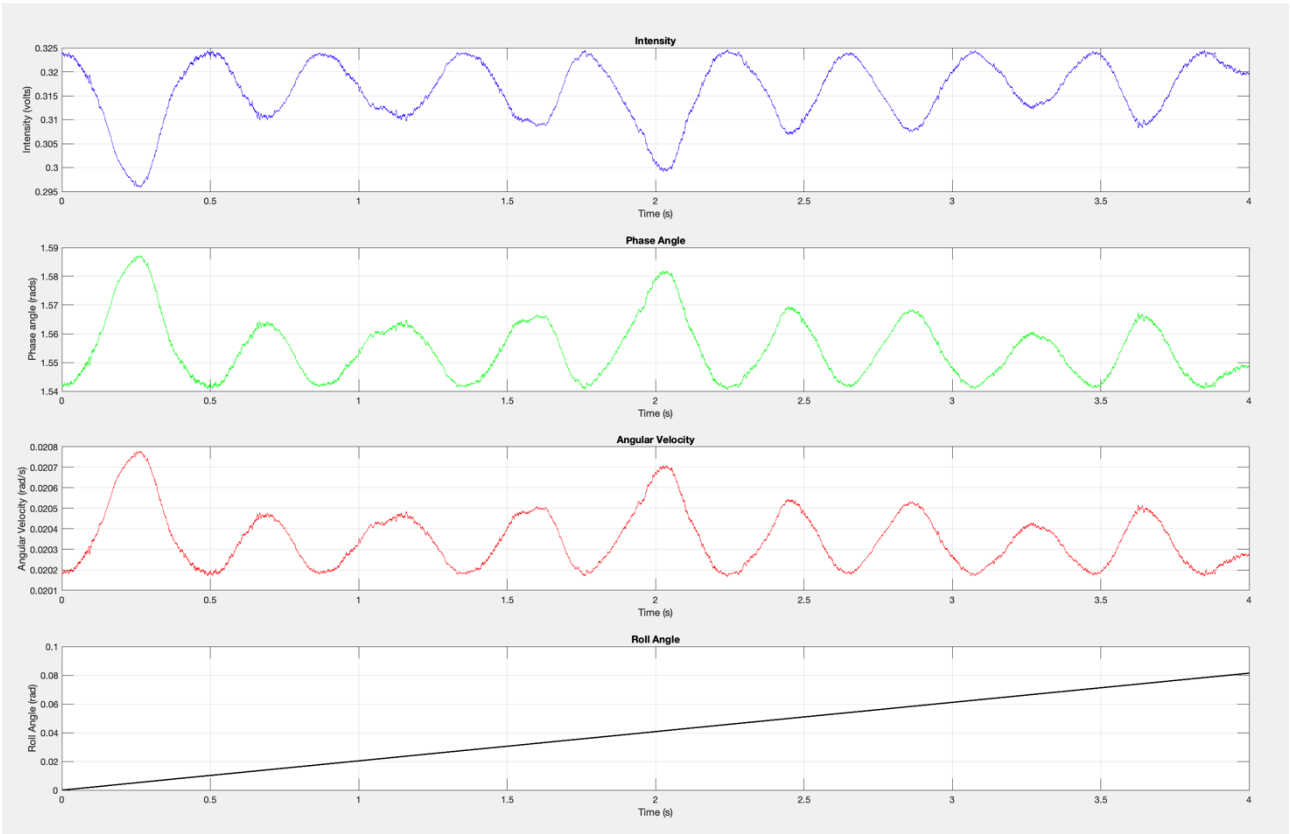Figure 23 – oscillations for 10 seconds
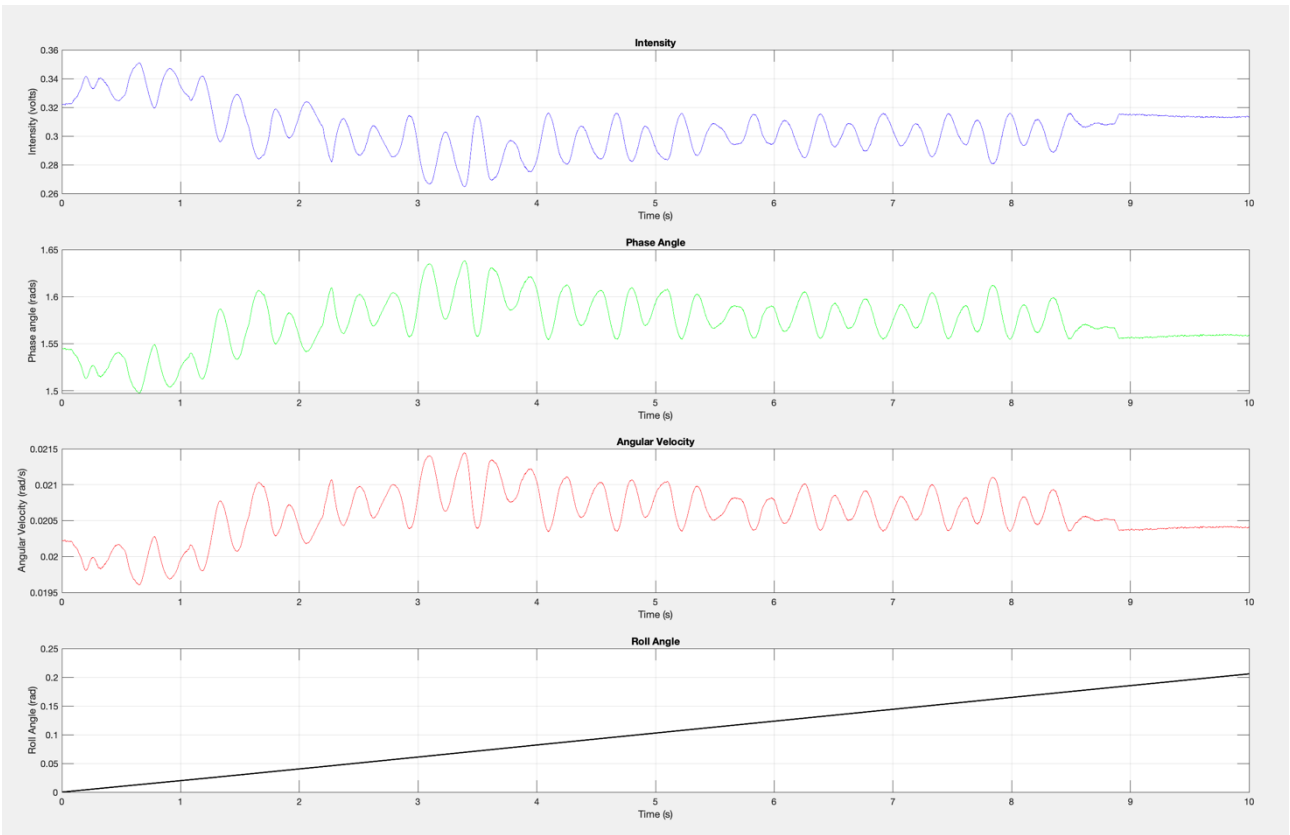
Figure 24 – fast oscillations for 4 seconds

Figure 25 – Fast oscillations for 10 seconds

$$\Delta\Phi = \cos^{-1}\frac{(I-I_0)}{I_M} \tag{12}$$

where: $\Delta\Phi$ is the change in phase angle (rad)

   I is the intensity (volts)

   I_0 is the base or initial intensity (volts)

   I_M is the amplitude of intensity variation (volts)

$$\omega = \frac{\lambda \times \Delta\Phi \times c}{2 \times n_f \times L^2} \tag{13}$$

where: ω is the angular velocity (rads/s)

   λ is the wavelength of the laser (m)

   c is the speed of light (m/s)

   n_f is the refractive index variation

   L is the length of the fibre optic cable (m)

The mean and standard deviation were calculated using the MATLAB code [Appendix A]. Since the roll angle was inaccurate, the values for mean and standard deviation are also inaccurate and cannot be used to evaluate the precision of the interferometer.

8   Conclusions and further work

An unforeseen circumstance arose from the system's inability to detect rotation, therefore hindering the ability to calculate the roll angle accurately and rendering it incapable of calculating accurate standard deviations and mean for the roll angle calculated. Analysis of relevant reports led to the conclusion that the Sagnac interferometer would have the capability to detect rotation based on the fringe patterns observed during rotational movements. If the system was to be improved, quadrature detection would be added to it, which introduces a phase shift of 90 degrees to of the signal, as shown in Figure 26 [29]. When you introduce this phase shift you basically shift the interference pattern and create two waves that are in about 90 degrees out of phase with each other. Through thorough analysis of these two waves, you can determine the direction and magnitude of the roll angle [30] [31].
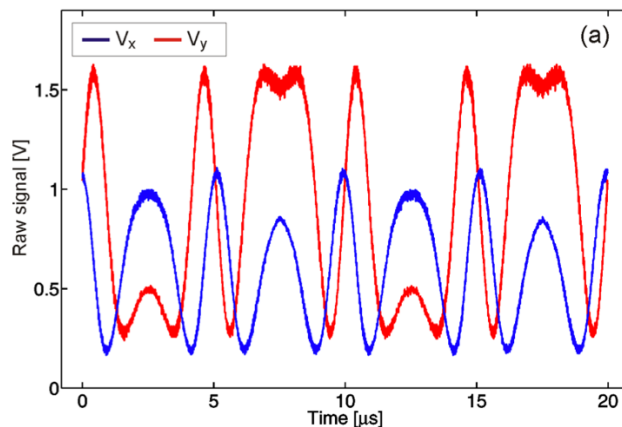

Figure 26 – shows the signals that are 90 degrees out of phase [31]

Wolfson School of Mechanical, Electrical and Manufacturing Engineering

Future work for this project would include but is not limited to introducing quadrature detection to the system, potentially designing, and developing and rotating motor that can be fixed to the fibre optic reel instead of the torsional pendulum. The frequency of a DC motor can be varied easily compared to the pendulum which makes it easier to calibrate the interferometer and makes the measurements from the interferometer more reliable. With regards to detection, it could be made autonomous with the integration of few sensors and a Bluetooth module.

This project has produced a working interferometer that can determine the axial rotation of the object. The only limitations of this would be that the calculation of roll angle is not autonomous and the interferometer's inability to detect direction. The core of the roll angle calculating procedure has been produced, however, there wasn't enough time to fix the unforeseen issues with the procedure, which meant that it did not work properly. Whilst falling short of producing a fully working system, the work carried out can provide a solution that can successfully determine the axial rotation in one direction.

The final desired outcome of this project is to create a system that utilizes optical sensors to measure axial rotation of an object. Addition of quadrature detection and developing a system to make the measurement of roll autonomous would be very beneficial to this project and would provide the fundamental bridge between the MATLAB code and the interferometer.

Appendix

Appendix A: MATLAB code

```
%% Calculating Phase

IM = 0.3089 + 0.306;
I0 = 0.306;
delta_phase = acos((I - I0)./IM);

%% Calculating Angular Velocity

lambda = 1310e-9;
r = 10e-2;
nf = 1.5;
length = 100;
omega = (lambda*delta_phase*physconst('lightspeed'))/(2*nf*(length)^2);

%% Smoothing the signals

smoothed_signal1 = movmean(I, 1000);
smoothed_angle = movmean(delta_phase, 1000);
smoothed_signal2 = movmean(omega, 1000);

%% Calculating angle of rotation

roll = cumtrapz(t, smoothed_signal2);

%% Calculating the mean and standard deviation of the roll angle

mean_angle = mean(roll);
std_deviation_angle = std(roll);
disp(['Mean angle: ', num2str(mean_angle)]);
```

```
disp(['Standard Deviation: ', num2str(std_deviation_angle)]);

%% Plotting the graphs

figure;
subplot(4,1,1);
plot (t, smoothed_signal1, 'b', 'LineWidth', 0.5)
grid;
xlabel('Time (s)');
ylabel('Intensity (volts)');
title('Intensity');

subplot(4,1,2);
plot (t, smoothed_angle, 'g', 'LineWidth', 0.5)
grid;
xlabel('Time (s)');
ylabel('Phase angle (rads)');
title('Phase Angle');

subplot(4,1,3);
plot (t, smoothed_signal2, 'r', 'LineWidth', 0.5)
grid;
xlabel('Time (s)');
ylabel('Angular Velocity (rad/s)');
title('Angular Velocity');

subplot(4,1,4);
plot (t, roll, 'k', 'LineWidth', 1.5)
grid;
xlabel('Time (s)');
ylabel('Roll Angle (rad)');
title('Roll Angle');
```

Acknowledgements

References

[1] B. F. I. H. S. K. Zembaty Z, "Rotation Rate Sensors and Their Applications," Sensors, Basel, 2021 Aug 7.

[2] L. J. Z. X. F. K. H. C. W. X. Y. X. Mi J, "Roll Angular Rate Measurement for High Spinning Projectiles Based on Redundant Gyroscope System," Micromachines, Basel, 2020 Oct 16.

[3] D. K. John Geen, "New iMEMS Angular- Rate-Sensing Gyroscope," ADI Micromachined Products Division, 2003.

[4] X. L. a. H. Z. Jiazhen Lu, "Tilt measurement using inclinometer based on redundant configuration of MEMS accelerometers," IOP Publishing Ltd, Beijing , 2018.

[5] J. Gehring, "GRAVITY INCLINOMETERS," *The Tool Shed,* vol. Number 120, 2002.

[6] S. J. D. J. M. J. W. Hamed Arianfard, "Sagnac interference in integrated photonics," 1 March 2023.

[7] M. H. Daniel, Advanced Optical Instruments and Techniques, Florida: CRC Press, 2018.

[8] G. Sagnac, "On the Proof of the Reality of the Luminiferous Aether," 1913.

[9] G. B. Malykin, "The Sagnac effect: correct and incorrect explanations," Uspekhi Fizicheskikh Nauk and Russian Academy of Sciences, 2000.

[10] J.-P. Liu, T. Tahara, Y. Hayasaki and T.-C. Poon, " Incoherent Digital Holography: A Review," 2018.

[11] Y. W. L. Z. B. W. P. Y. Xiangwei Liu, "High-precision dynamic measurement of roll angle based on digital holography," ptics and Lasers in Engineering, 2023.

[12] X. Z. F. W. R. X. W. W. S. L. M. X. He Yuan, "Accurate reconstruction for the measurement of tilt surfaces with digital holography," Optics Communications, 2021.

[13] T. R. L. M. P. F. Vito Pagliarulo, "Numerical tools for the characterization of microelectromechanical systems by digital holographic microscopy," 2015.

[14] T. O. M. K. C. K. M. S. a. A. M. K. Tobita, "A rotary encoder based on magneto-optical storage," 2005.

[15] G. Y. H. L. Y. B. Y. S. L. Y. B. L. Xuan Li, "A novel optical rotary encoder with eccentricity self-detection ability," 2017.

[16] E. Hecht, "Interference," in *Optics (First Edition*, pearson, 1974.

[17] B. Culshaw, "The optical fibre Sagnac interferometer: an overview of its principles and applications," IOP Publishing Ltd, 2005.

[18] P.Hariharan, "The Laser as a light source," in *Basics of Interferometery*, Sydney, School of physics, University of Sydney, 2006, pp. 39-43.

[19] B. T. M. V. A. H. K. T. V. Grattan, "Single Mode optical fibre sensors," in *Optical Fibre sensor technology*, London, EM Technology, pp. 85-90.

[20] W. Spottiswoode, Polarisation of light, London: Macmillan and co., 1895.

[21] W. Moebs, University Physics (volume 1), Pressbooks, 2016.

[22] R. C. PP Benham, Mechanics of Engineering Materials, Essex: Pearson, 1996.

[23] D.-H. K. a. J. U. Kang, "Sagnac loop interferometer based on polarization maintaining photonic crystal fiber with reduced temperature sensitivity," Department of Electrical and Computer Engineering, The Johns Hopkins University, Baltimore, 2004.

[24] S. T. H. W. T. M. a. H. H. Kenji Wada, "Pulse-shaping of gain-switched pulse from multimode laser diode using fiber Sagnac interferometer," Optical Society of America, Osaka, 2008.

[25] S. CORPORATION, "High Performance Tunable Laser (TSL-510)," SANTEC CORPORATION, 2014.

[26] E. Neumann, Single Mode Fibres - Fnndamentals, Berlin: Springer-Verlag Berlin Heidelberg, 1988.

[27] "ThorLabs," ThorLabs, [Online]. Available: https://www.thorlabs.com/thorproduct.cfm?partnumber=SMF-28-100.

[28] "THORLABS," ThorLabs, [Online]. Available: https://www.thorlabs.com/thorproduct.cfm?partnumber=PDB470C-AC.

[29] S. G. I. M. Q. H. a. T. K. Taeho Keem, "Removing nonlinearity of a homodyne interferometer by adjusting the gains of its quadrature detector systems," Optical Society of America, 2004.

[30] S. G. I. M. Q. H. a. T. K. Taeho Keem, "Simple, real-time method for removing the cyclic error of a homodyne interferometer with a quadrature detector system," Optical Society of America, 2005.

[31] T. P. a. J. M. Peter Gregorčič, "Quadrature phase-shift error analysis using a homodyne laser interferometer," Optical Society of America, 2009.

[32] "NCBI," [Online]. Available: [https://www.ncbi.nlm.nih.gov/pmc/articles/PMC8402159/.

[33] F. Lozano, S. Emadi, S. Komarizadehasl, J. Arteaga and Y. Xia, "Enhancing the Accuracy of Low-Cost Inclinometers with Artificial Intelligence," Barcelona, 2024.